Radiative transitions in undoped and Mn-doped $CdGeP_2$ crystals

Gennady Medvedkin
General Molded Glass, Inc., Torrance, California 90502, USA

(Received 27 February 2024; revised 4 May 2024; accepted 13 May 2024; published 28 May 2024)

New radiative transitions in undoped and Mn-doped $CdGeP_2$ crystals have been detected by low-temperature photoluminescence and excitation at different wavelengths. $CdGeP_2$ is a direct-band-gap semiconductor with good luminescent properties due to intrinsic point defects, mainly V_{Cd} and V_P vacancies, Cd_{Ge}, Ge_{Cd}, and Ge_P cation antisites, and defect pairs. Doping with manganese does not significantly affect the intrinsic defects but cardinally changes the emission at energies above the band gap. Optical transitions occur due to redistribution of optical energy channels through Mn ions embedded in the tetragonal lattice, which allows observation of previously unobserved interband transitions in $CdGeP_2$ crystal. The emission at energies of 2.5–3.5 eV becomes even stronger than the emission through intrinsic point defects, especially when deep levels are excited by violet (325 nm) and blue (458 nm) lasers compared to green (514, 532 nm) lasers.

DOI: 10.1103/PhysRevB.109.205206

I. INTRODUCTION

Ternary II-IV-V_2 diamondlike semiconductors are the closest cationic analogs of II-VI and anionic analogs of III-V binary semiconductors. Upon doping with Mn, crystals II-VI become antiferromagnetic, while crystals III-V and II-IV-V_2 switch to the ferromagnetic state. $CdGeP_2$ belongs to the direct-band-gap semiconductors and, compared, for example, with pseudodirect semiconductors $ZnGeP_2$ or $ZnSiAs_2$, shows good emissivity.

$CdGeP_2$ (CGP) single crystal is one of the effective materials for laser energy conversion in the terahertz range [1,2]. The Mn-doped material was the first ferromagnetic semiconductor with diamondlike crystal structure and Curie temperature above room temperature, $T_C = 318-320$ K [3–6]. Optoelectronic properties of $CdGeP_2$ include high photosensitivity, strong luminescence, optical anisotropy in the near-IR and visible ranges, nonlinear optical efficiency, realization of both *n*- and *p*-type conductivity, and creation of *p*-*n* junctions and heterojunctions with III-V binary analogs such as $CdGeP_2$/InP [7]. The lattice constants of chalcopyrite $CdGeP_2$ are $a = 5.741$ Å, $c = 10.775$ Å. The direct gap ($E_g = 1.73$ eV at 300 K; 1.84 eV at 80 K) together with the edge optical dichroism put this material among the potentially attractive materials for solar cells, polarization sensors, and other photovoltaic devices [8–12]. Room-temperature ferromagnetism in $CdGeP_2$:Mn offers great potential for spintronics based entirely on diamondlike materials [13,14].

However, the luminescent properties of $CdGeP_2$ were reported rather sparingly in the literature [15–18]. Point defects have been investigated by electron paramagnetic resonance (EPR) and optical absorption and identified as charged states that undergo optical quenching [19]. The fundamental absorption edge in $CdGeP_2$ crystals is affected by shallow and deep levels of defects, and at high acceptor-donor N_A/N_D compensation, the Urbach tail is significantly extended by 0.4 eV [20,21]. Deep defect levels in chalcopyrite were modeled theoretically [22], and electron traps known as "DX centers" were simulated for the ternary analogs $CuInSe_2$ and $CuGaSe_2$. The defect physics has been intensively investigated by modeling techniques for $CuInSe_2$ [23] and $ZnGeP_2$ [24–27]. Thus, the problem of radiative transitions in $CdGeP_2$ through defect centers and *d*-element centers remains an important experimental task in the study of the fundamental optical properties of both absorption and emission.

II. EXPERIMENTAL DETAILS

$CdGeP_2$ single crystals were grown by the directional crystallization method. No intentional doping or deviation from stoichiometry was performed during synthesis and growth (Ioffe Physical Technical Institute). Mn doping was performed in a molecular beam epitaxy chamber (Tokyo University of A&T) by deposition and diffusion of metallic manganese. Although annealing $CdGeP_2$ crystals at T = 600° C–700° C can move defect levels to lower energies by 20–80 meV, the lower temperatures <510° C do not significantly affect the emission bands in photoluminescence (PL) spectra [17]. Therefore, we used the low-temperature annealing (LTA) condition for Mn diffusion, $T_{dif} = 500°$ C.

Detailed x-ray diffraction patterns were measured in Refs. [4,5], and the analysis showed that the structure of the Mn diffusion layer is single crystal. The interplanar spacing and lattice constants decrease with increasing manganese concentration: $a = 5.741$ Å $\rightarrow 5.710$ Å $\rightarrow 5.695$ Å in the series of compounds $CdGeP_2 \rightarrow Cd_{1-x}Mn_xGeP_2 \rightarrow Cd_{1-y}Mn_yGeP_2$ ($x < y$) [4]. The profile of manganese atoms in the specimen followed the exponential decay characteristic of diffusion distribution. The concentration ratios of chemical elements were measured using a field emission scanning electron microscope [3,4]: Mn/Cd = 0.52, Mn/Ge = 0.28 (top layer $d \sim 100$ nm); Mn/Cd = 0.2, Mn/Ge = 0.1 (400 nm); Mn/Cd = Mn/Ge = 0 (2.6 μm, concentration detection limit). The high-resolution x-ray diffraction on (112) and (008) reflexes gave three-dimensional (3D) information

about ordering in Mn-doped $ZnGeP_2$ [5]. Magnetic and magneto-optical properties are described in Refs. [4–6].

The low-temperature PL measurements in this work were performed at $T = 16$ K in a He cryostat. Temperatures of 10, 20, and 80 K were also used for supplementary measurements. We selected the temperature $T = 16$ K to get true information about the phosphorus vacancy defect $V_P^0 \leftrightarrow V_P^+$, whose behavior at temperatures below 18 K is known [19]. PL spectra were taken in two independent laser setups with different laser pumping to compare the PL emission parameters (peak, intensity, FWHM, etc.) of undoped crystals and crystals after the doping procedure. Laser excitations with two wavelengths $\lambda_1 = 458$ nm (Ar laser) and $\lambda_2 = 325$ nm (HeCd laser) were used. The light powers of the laser sources were 40 and 15 mW, respectively. A low-frequency phase lock-in amplifier detector with FEU-62 and FEU-100 photomultiplier tubes (PMTs) was used. The FEU-100 PMT with high sensitivity $S_a = 100$ A/lm and spectral nonuniformity of about two orders of magnitude in the range 180–780 nm was used in the HeCd laser setup. To eliminate the nonuniformity, the PMT photoresponse was corrected by normalization to the PL_{CMGP}/PL_{CGP} ratio. In contrast to PL measurements with green-line excitation at 514 and 532 nm [15], this work investigates the blue-violet laser pumping at 458 and 325 nm. Excitation by photons of higher energy allows reliable generation of radiation from deep levels, including intracenter transitions in Mn ions.

III. RESULTS

A. Photoluminescence excitation, 458 nm

We performed PL measurements at $T = 16$ K, since antisite and vacancy defect centers in $CdGeP_2$ easily transition from one charge state to another at temperatures below 18 K and under the influence of $\lambda = 700$ and 850 nm light [19]. This particular temperature was recently determined from EPR measurements of $CdGeP_2$ [19]. Neutral V_P^0 phosphorus vacancies are only formed by light near the band edge (~ 670 nm) when the crystal is at $T \approx 18$ K or below. V_P^0 donors are unstable at such low temperatures and revert to the single ionized charged V_P^+ state when the light is turned off [19]. Thus, the temperature of 16–18 K is an important starting point for studying these defects. The process, known as optical quenching, was observed in optoelectronic transients in II-VI and many other semiconductor compounds. In addition, the temperature conditions for PL (16 K) and EPR (18 K) are similar, thus taking advantage of data pooling.

Figure 1 shows PL spectra of the undoped and Mn-doped crystals peaking at 1.33 and 1.546 eV, respectively. All PL maxima recorded under Ar-laser excitation (2.71 eV) are located below the band-gap energy of $CdGeP_2$. Radiative recombination in undoped crystals defines optical transitions through point defect levels at 1.16, 1.33, 1.46, and 1.55 eV. In Mn-doped crystals, the same PL peaks of different intensities indicate that Mn has a strong influence on intrinsic defects only to redistribute the intensities of the peaks, but does not affect their energy positions. The energy position of the PL peaks is consistent with that observed previously in $CdGeP_2$ [15]. LTA is known for $ZnGeP_2$ to improve the crystal

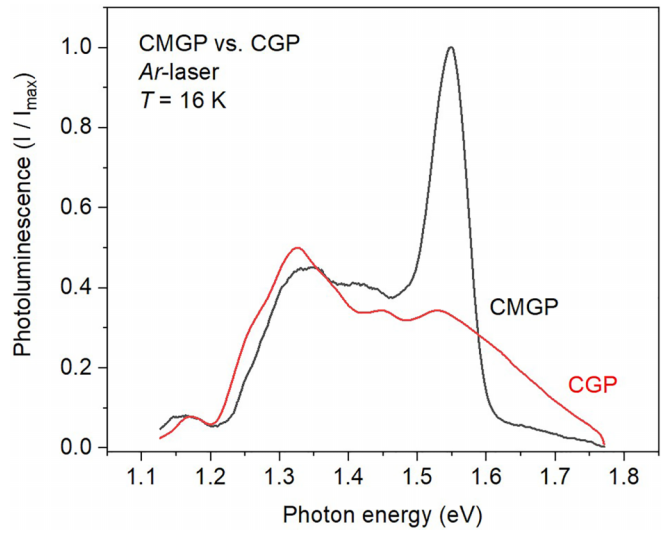

FIG. 1. PL of $CdGeP_2$ crystals: undoped as grown (red line) and Mn doped (black line). The undoped crystal was not heat processed prior to diffusion.

structure and optical properties [28]; the same is observed for photoluminescence of $CdGeP_2$ after the thermal diffusion at 500° C. The dominant emission in the Mn-doped crystal at 1.55 eV is due to the transition through the acceptor level created by the V_{Cd} vacancy.

Below we show that the Ge_{Cd} donor defect is also involved in the donor-acceptor (D-A) transition with V_{Cd}. This emission exists in both crystals, but in the undoped one with much lower intensity. PL and optical absorption at this energy have also been observed at $T = 80$ and 10 K in undoped, Mn-doped, Ga-doped, and In-doped materials and after recrystallization of glassy $CdGeP_2$ at 500° C [15–18]. It dominates after Mn doping for short-term LTA and after glass recrystallization for long-term LTA, annealing in ampoules filled with powdered $CdGeP_2$ compound in Cd or P vapors at 700°C [17]. Thus, it can be concluded that all the above cases are mainly due to intrinsic defects rather than impurities. The dominant point defects in $CdGeP_2$, similar to $ZnGeP_2$, are V_{Cd} and V_P vacancies, Ge_{Cd} and Cd_{Ge} cation antisites, and defect pairs. LTA processing affects the point defect ensemble more prominently than doping, since the concentration of intrinsic point defects in II-IV-V_2 crystals is very high, ranging from 10^{17} to 10^{20} cm^{-3}. Simulations performed for $ZnGeP_2$ [24] estimate the density of antisite defects in different charge states to be 10^{17}–10^{18} cm^{-3}, and $>10^{14}$ cm^{-3} for the V_{Zn} vacancy. This range and minimum threshold are clearly underestimated because V_{Zn} is the dominant defect in the crystal, and the modeling contradicts the experimental results of many groups [19,29–31]. Other simulations [25–27] give a much better estimate of the density of states (DOS) for the defect complex (V_{Zn}-Ge_{Zn}-V_{Zn}), which is rather compatible with the DOS in an ideal crystal and consistent with experiments. Thus, we attribute the emission at 1.55 eV to a radiative transition involving acceptor V_{Cd} and donor Ge_{Cd} defects.

Doping with Mn leads to enhancement and broadening of a number of emissions detected in this work. The most intense peak at 1.335 eV and a secondary peak at 1.44 eV in Fig. 1

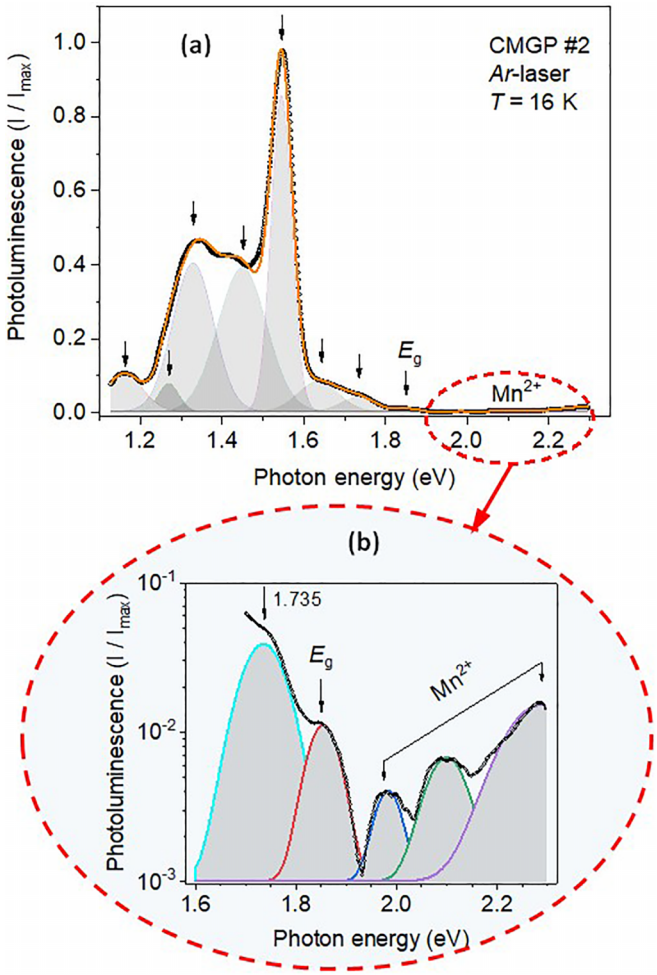

FIG. 2. (a) PL of Mn-doped $CdGeP_2$ crystal. Shaded contours are Gaussian deconvolution for bands in the impurity spectral region. They resolve into seven distinct intrinsic defect bands under Ar-laser excitation. (b) The enlarged inset shows PL bands for interband (E_g) and intracenter (Mn^{2+}) transitions.

were observed in both undoped and In- and Cu-doped crystals [17], so it is obvious that these bands are due to intrinsic (and not impurity) causes. The observed emission bands can be attributed to the predominant intrinsic defects affected by LTA, such as V_P vacancy and Ge_{Cd} antisite. These point defects are metastable and their charge state can be switched by IR backlighting at specific wavelengths [19]. There is evidence that LTA improves the local crystal ordering in $ZnGeP_2$, confirmed by optical dichroism measurements [28].

Due to the manganese impurity and blue-violet excitation, deeper radiative transitions take effect. As the excitation photon energy increases (from green to blue), the optical radiative transitions from higher energy levels become more distinct, as shown in the magnified view in Fig. 2(b). In addition, the new emission transitions become more intense when the excitation photon energy is further changed [from blue to violet; see Fig. 3(a)]. We used the spectral deconvolution method to extract individual emissions from the obtained PL spectra, assuming that each individual emission can be expressed by a uniformly broadened spectral band. Nonlinear multipeak fitting involved a Gaussian function of the form

$$I = I_0 + \frac{A}{w\sqrt{\pi/2}} \times \exp\left[-\frac{2(\hbar\omega - \hbar\omega_0)^2}{w^2}\right], \qquad (1)$$

where I_0 is the baseline offset, A is the total area under the spectral curve from the baseline, $\hbar\omega_0$ is the center of the peak, and w is 2σ, approximately 0.85 times the width of the band at half height. The standard deviation σ is used to calculate the full width at half maximum (FWHM),

$$\mathrm{FWHM} = 2\sigma\sqrt{2\ln 2} \approx 2.3548\sigma. \qquad (2)$$

The results of the multipeak Gaussian fitting are shown in Fig. 2, with arrows in Fig. 2(a) indicating seven extrinsic (point defects and/or impurities) peaks and one intrinsic (E_g) peak. The high-energy part is observed with significantly reduced intensity, while the low-energy part is consistent with previously observed PL from (Cd, Mn)GeP_2 layers and $CdGeP_2$ layers epitaxially grown on GaAs [15].

Highly sensitive, precise measurements and careful analysis of PL spectra near the band gap allowed identification of weak emission peaks associated with intracenter transitions in Mn^{2+} ions. Figure 2(b) shows that the energy of these emissions exceeds the value of E_g and can be confidently observed under blue and/or violet laser excitations. In fact, we used different excitation wavelengths to retrieve information from different depths of the diffusion layer $CdGeP_2$:Mn. The Mn concentration in our specimen was as follows: surface, Mn/Cd = 0.534; top layer ($d \approx 0.1\,\mu$m), Mn/Cd = 0.52 and Mn/Ge = 0.28; depth ($d = 0.4\,\mu$m), Mn/Cd = 0.2 and Mn/Ge = 0.1; depth ($d = 0.6\,\mu$m), Mn/Cd = 0.12 and Mn/Ge = 0.06; and full thickness (2.6 μm), Mn/Cd = Mn/Ge = 0. The region excited by the violet laser corresponds to a thin top layer with maximum Mn concentration, while the green laser penetrates deeper and brings information from the region with lower Mn concentrations.

The most intense emissions are observed in the photon energy range 1.1–1.8 eV (Fig. 2). The dominant peak was accurately recorded at 1.546 eV in the Mn-doped crystal, and the intensity of this peak is three times higher than in the undoped crystal (Fig. 1). We attribute this enhancement in $CdGeP_2$:Mn to the fact that LTA improves the local crystal structure as in $ZnGeP_2$ [28] with simultaneous substitution of Mn atoms on Ge sites [32–34]. In particular, Ge_{Cd} sites are impacted and can form additional complexes ($2V_{Cd}$-Ge_{Cd}) that have low formation energies [25]. Thus, we attribute this radiative transition to the D-A transition $Ge_{Cd} \rightarrow V_{Cd}$. Note that the emission transition energy of 1.55 eV corresponds to the photon wavelength interval from 700 to 850 nm, where optical quenching in the EPR signal was observed [19]. Group-IV to group-II antisites are the major donors in II-IV-V_2 phosphides [19] because their formation energy is the lowest [25]. The V_{Cd} vacancy was found to be the most abundant point defect in undoped $CdGeP_2$ [19], and it is present in high concentration ($N_A > 10^{18}\,\mathrm{cm}^{-3}$) in as-grown crystals. Thus, the introduction of Mn into the chalcopyrite lattice impacts the formation of D-A pairs and complexes. The lowest-energy emission with a peak at 1.16 ± 0.01 eV [Fig. 2(a)] has a relatively low intensity. Its spectral position coincides with the optical absorption band at 1.18 eV (80 K) [19].

Although interband optical transitions in II-IV-V_2 undoped semiconductors can be observed in PL only at low temperatures and at very low free charge concentration, such as in the excitonic PL of p-$CdSnP_2$ [35], here we found an unusual doping effect of Mn leading to the appearance of high-energy radiative transitions above E_g. The optical effect is known in CdMnTe crystals [36], where the band gap increases upon Cd → Mn substitution, and PL peaks were found at energies greater than the E_g of CdTe crystal. However, the binary solid solution CdMnTe is not ferromagnetic, unlike (Cd, Mn)GeP_2, which is a room-temperature ferromagnetic. This effect was first detected in the ferromagnetic diamondlike material [3].

While the PL emission near E_g is not observed in heavily doped or compensated material, Mn impurity stimulates the rearrangement of the defect ensemble in $CdGeP_2$. Radiative transitions through intrinsic defect centers in the band gap remain at the same positions, but with different intensity. Transitions above the band gap get into continuum bands and electrons relax to the bottom of the conduction band (CB) and then recombine with holes from the valence band (VB). The mechanism is similar to Mn-doped II-VI compounds, where the main PL peak shifts with [Mn] from E_g (CdTe) to $E = 2.0$ eV (first Mn^{2+} intracenter transition) [36,37]. However, in $CdGeP_2$:Mn two sets of transitions are observed, as shown in Fig. 2. The appearance of ferromagnetism in Mn-doped $CdGeP_2$, as we believe, occurs by a mechanism similar to that for GaAs or GaP. The minor substitution Ge → Mn in $CdGeP_2$ occurs in the same way as Ga → Mn in GaAs, and the Mn_{Ge} acceptor creates two free holes, in contrast to the Mn_{Ga} acceptor, which has only one hole in III-V compounds. Exchange between d levels of Mn^{2+} ions and p-like top levels in the VB of $CdGeP_2$ has to be similar to GaAs, but the great advantage is the high Curie temperature, $T_C = 310-355$ K, in various II-IV-V_2 compounds [6]. The observed radiative transitions in Mn-doped $CdGeP_2$ confirm the double heterovalent mechanism "substitute and dope," a specific mechanism for II-IV-V_2 chalcopyrites.

Radiative transitions at energy E_g arise between the CB and VB, and emission at energies above E_g is associated with intracenter Mn^{2+} transitions. The intracenter transitions in Mn^{2+} ions in structures with tetrahedral crystal field occur between the excited electronic levels $^4T_1(^4G)$, $^4T_2(^4G)$, $^4A_1(^4G)$, and $^4E(^4G)$ and the ground level $^6A_1(^6S)$ [36]. The symmetry of Mn^{2+} centers in the crystal structures of sphalerite and chalcopyrite is similar due to the tetrahedral coordination of atoms and the quasicubic model approach for chalcopyrite [38]. Thus, the energy splitting diagram of the lowest excited state of the $3d^5$ level (^4G) relative to the ground state (^6S) for the Mn^{2+} ion [36] can be used in chalcopyrite. Nevertheless, this phenomenon is different from that known in III-V and II-VI compounds, since II-IV-V_2 compounds combine two mechanisms, "substitute and dope," in one ternary compound. The double action was confirmed by EPR, which detected two different states of Mn ions in chalcopyrite [39], and by theory [32]. The hybridization of valence-band electrons with d states localized on the transition metal can be considered as a self-sustaining mechanism to explain hole-mediated ferromagnetism in II-IV-V_2 chalcopyrites.

There is evidence for hole-mediated ferromagnetism. Modeling [32] predicts that Mn_{Ge} would be the acceptor and ferromagnetism results from the interaction of Mn with hole-producing intrinsic defects. A hole transport experiment in $Zn_{1-x}Mn_xGeP_2$ evidences the p-type conductivity with a half-metallic character due to the temperature dependence of resistivity [33,34]. Band-structure calculations of $Cd_{1-x}Mn_xGeP_2$ render the material half-metallic and confirm the carrier-induced ferromagnetism [40,41].

In addition, isolated Mn centers and nanoclusters have been detected by EPR [39], magnetotransport, and giant electron spin echo measurements [33,34,42] in (Zn, Mn)GeP_2 and simulated for $CdGeP_2$:Mn and $ZnGeP_2$:Mn [43]. The nanocluster formation in diamondlike compounds occurs in similar way since it is governed by the tetrahedrally coordinated cation-anion bonds and nanoclusters of P_2-Mn-P_2 and As_2-Mn-As_2 type are created in both II-IV-V_2 and III-V compounds, e.g., in GaP:Mn [44–48] and GaAs:Mn [49–51]. Therefore, radiative transitions (Figs. 2 and 3) can occur through Mn^{2+} cationic antisites, Mn^{2+} nanoclusters, or isolated Mn^0 interstitials. We attribute this emission to intracenter Mn^{2+} transitions because most of the manganese ions are embedded in cation sublattices.

B. Photoluminescence excitation, 325 nm

Figure 3 shows the PL spectrum of Mn-doped crystal under violet line excitation, where emission dominates at higher energies $>E_g$. The curve was normalized by the PL signal ratio in Mn-doped and undoped crystals to get the relative quantum efficiency over the broad spectral range 350–600 nm (2.1–3.5 eV). The resolved bands are given in grey as uniform Gaussian lines. The main bands are associated with transitions in Mn centers.

The local crystal structure around Mn^{2+} ions in $CdGeP_2$ crystal was improved by LTA and diffusion processing at 500° C. Similar LTA was applied to undoped $ZnGeP_2$ [28] and resulted in improved local order in the defect ensemble. The introduction of the d element presumably increases the concentration of Ge-Cd antisites due to Mn^{2+}_{Ge} acceptors. Manganese atoms displace germanium atoms from their inherent Ge_{Ge} sites to Ge_{Cd} antisites and interstitials in accordance with the Pauling electronegativity difference.

The emission peak at 1.64 eV agrees well with the absorption band at 1.64 eV [19], and minor emission is observed at 1.735 eV [Fig. 3(b)]. These bands are associated with point defects Ge_{Cd} and V_{Cd}. The interband transition at 1.85 eV corresponds to the band gap E_g at $T = 16$ K (this value will be defined below). All observed emissions with energies above E_g are related to intracenter transitions in Mn^{2+} ions. Since the Mn_{Ge} dopant creates an excess of holes, being an effective acceptor, the electrical conductivity of $CdGeP_2$:Mn increases and hole-mediated ferromagnetism takes effect at room temperature, similar to $ZnGeP_2$:Mn and (Zn, Mn)GeP_2 [3–5,32–34,40,42]. Thus, hole transfer between Mn^{2+} ions and/or nanoclusters and the crystal matrix occurs quite easily.

C. Temperature dependence of the band gap

The energy band gap of $CdGeP_2$ was not measured before at $T = 16$ K, so we used the Varshni formula $E_g = E_0 - \alpha T^2/(T + \Theta)$ [52] to fit the calculated curve to the

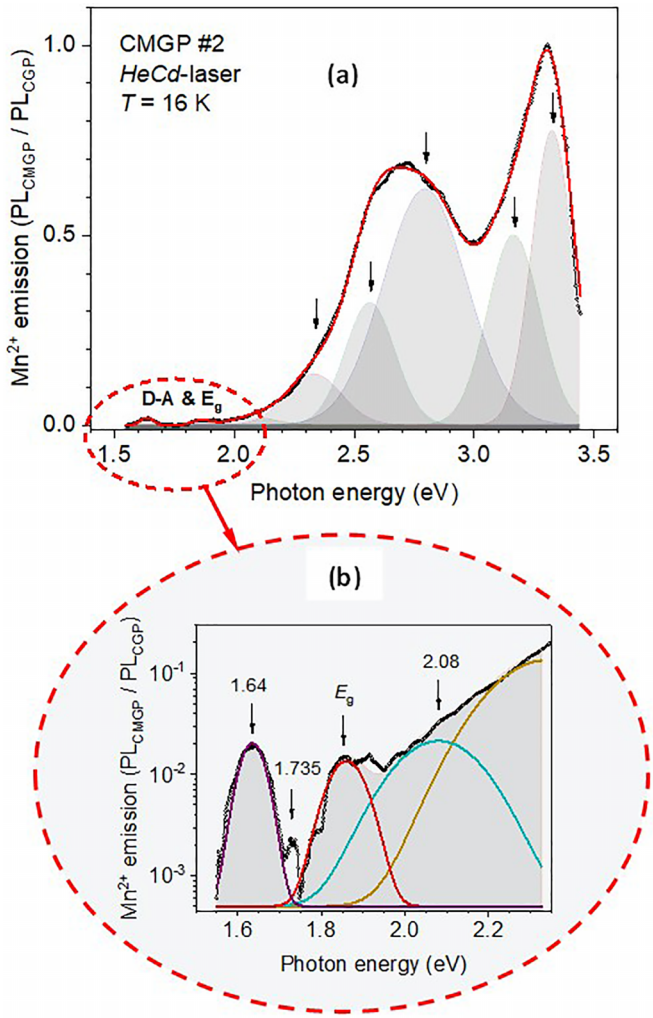

FIG. 3. PL of Mn-doped $CdGeP_2$ crystal. Spectral distribution corresponds to relative quantum efficiency. (a) High-energy Mn^{2+} emissions at 2.0, …,3.5 eV allowed under HeCd laser excitation and (b) enlarged inset for D-A and interband (E_g) emissions.

available experimental data. Here E_0 is the value of the band gap at 0 K. The constants α and Θ are connected with the electron (exciton)–phonon interaction and Debye temperature, respectively.

Figure 4 gives the fitting of the Varshni formula to experimental points measured directly at the fundamental absorption edge in the temperature range 3.4–300 K. Experimental points were taken from optical absorption and oscillating transmission measurements carried out on very thin single-crystal plates (10 and 23 μm) [20,21]. Though the crystal had a heavy compensation $N_A/N_D = 0.6 - 0.9$ and the exponential Urbach tail can shift the E_g value towards lower energies by 30–60 meV, the characteristic spectral features in the absorption curve at $\alpha_0 = 2\times10^4\,\mathrm{cm}^{-1}$ [20] ensure the correct E_g value at $T = 80$ and 295 K. The Debye temperature for $CdGeP_2$ is $\Theta = 340$ K; it was calculated from the experimental specific heat capacity [53,54].

Experimental data from two independent measurements [20,21] demonstrate excellent agreement with each other. An accurate estimate gives the energy band gap of $CdGeP_2$ crystal

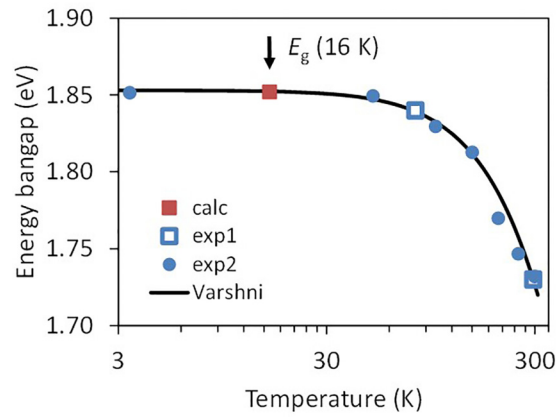

FIG. 4. Temperature dependence of the band gap in $CdGeP_2$. Blue dots, experiments 1 and 2 [20,21]; red dot, calculation; line, E_g (16 K) = 1.852 eV defined according to the Varshni formula.

as $E_g = 1.852$ eV at $T = 16$ K. This temperature is consistent with the experimental conditions of this work. The spectral analysis below also compares the data measured at $T = 10 - 20$ K, and allows to construct the energy-level diagram with the exact value of E_g.

D. Summary of photoluminescence emissions

The emission intensity in the defect or impurity region, near E_g, and in the Mn^{2+} transition region varied because of the different sensitivity of the PMTs in the broad spectral range (Fig. 3). To improve accuracy, we used multiple runs followed by smoothing of the collected data. The broad spectra obtained include many overlapping emission bands for each laser excitation wavelength. They are in good agreement with each other. The deconvolution method allowed us to perfectly reconstruct the individual emission bands as Gaussian bands according to Eq. (1). By applying nonlinear multipeak fitting (OriginPro 2018), we identified the spectral parameters for the individual emission bands and depicted them in 3D histograms (Fig. 5). The corresponding numerical data are collected in Table I. The temperatures $T = 16$ K and $T = 10$ and 20 K from [15] were also used in the present work to satisfy the narrow range of T and to perform the spectral analysis correctly.

The ensemble of intrinsic defects and Mn impurity centers was subjected to various excitations (from green to violet), resulting in contrasting spectral effects.

The three-dimensional histograms in Figs. 5(a)–5(d) are plotted for the following spectral parameters: emission band peaks, FWHM, maximum amplitudes, and radiative transition powers, respectively. For intrinsic point defects in crystals and epilayers pumped by green lasers (532 and 514 nm), five main emissions are known [15] and are shown in green [Fig. 5(a)]. These emissions occupy the interval $E < E_g = 1.85$ eV. High-energy pumping with blue (458 nm) and violet (325 nm) lasers excited a number of new emissions at peak energies above E_g. The position of the band gap in histograms is marked by arrows for both blue and violet pumping. For green-blue lasers, the uncertainty of the radiative transitions at low energies of 1.1–1.8 eV was $\Delta E = 20-60$ meV. This scatter can

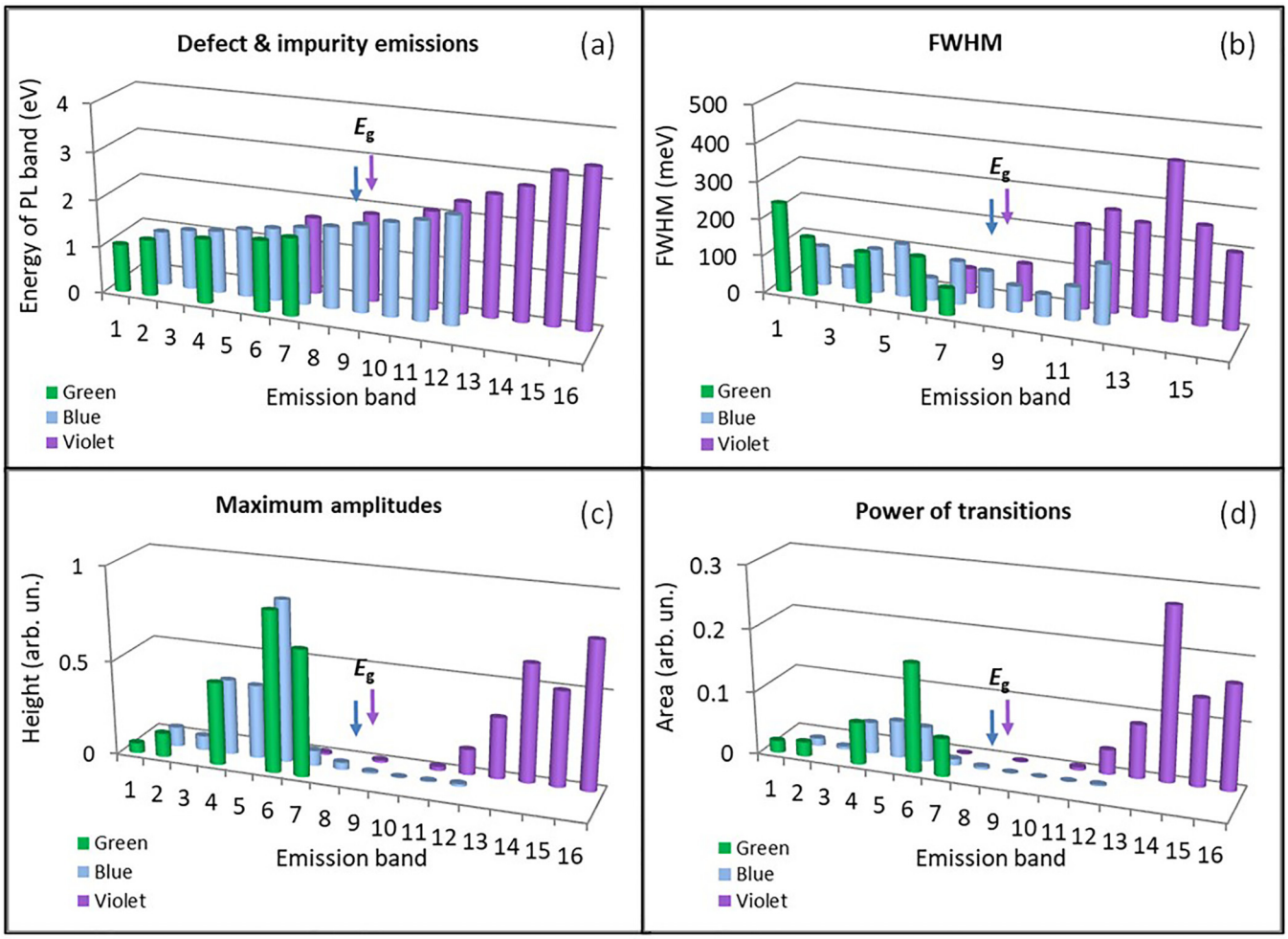

FIG. 5. Spectral parameters of emission bands in Mn-doped $CdGeP_2$ crystals. Emission bands 1 to 16 cover the spectral range 1.1–3.5 eV at $T = 16$ and 20 K. Colors correspond to the laser excitation: violet (325 nm), blue (458 nm), and green (532 nm).

TABLE I. Spectral parameters of emission bands in Mn-doped $CdGeP_2$ crystals. Ratios are given for blue/violet laser excitations. Center, FWHM, area, and height are obtained by nonlinear multipeak fitting for individual Gaussian bands.

Emission band	Center (eV)	FWHM (meV)	Area	Height	Defect[a]	Radiative transition
1	1.16	106	0.012	0.104	Ge_p^-	CB → A
2	1.27	59	0.005	0.076	V_P	D → VB
3	1.33	117	0.050	0.401	V_P	CB → A
4	1.45	141	0.059	0.389	Ge_{Cd}^+	D → VB
5	1.546	60	0.055	0.856	Ge_{Cd}, V_{Cd}	D → A
6	1.64/1.64	115/68	0.010/0.001	0.081/0.012	V_{Cd}	CB → A
7	1.735	100	0.004	0.038	Ge_{Cd}, V_{Cd}	D → A
8	1.85/1.86	71/100	0.001/0.001	0.010/0.013		CB → VB (E_g)
9	1.98	59	0.0002	0.003		Mn^{2+} intracenter
10	2.10/2.08	89/224	0.001/0.005	0.006/0.021		
11	2.29/2.34	159/271	0.002/0.039	0.014/0.134		
12	2.57	247	0.085	0.323		
13	2.80	412	0.272	0.620		
14	3.17	259	0.138	0.500		
15	3.33	200	0.165	0.774		

[a]Defect notation is given on the basis of the present work and data from Refs. [15,19].

be explained by the different concentrations of intrinsic point defects in the studied crystals and the large-scale rms potential modulating the edges of the energy gap due to fluctuations in the density of charged centers. While the spectral positions of the emission bands remain unchanged in the undoped material and after Mn doping, their intensity changes quite markedly. Green and blue excitations affect the near-IR spectral bands (1.1–1.8 eV), while violet light causes radiative recombination at 2.0–3.5 eV [see Fig. 5(a)].

The total number of resolved bands in the impurity region is seven, and the most intense bands are five, as can be seen in Fig. 5(c). The main emission is due to defects with a fairly stable energy position, so it can be concluded that the defect levels in the band gap of this II-IV-V_2 semiconductor do not shift much with λ excitation. However, at different pumping λ, optical energy is transferred through alternative channels: from the Mn center to the matrix, via point defect recharging and optical quenching. This markedly changes the network of optical transitions. Finally, the introduction of manganese makes visible emission that could not be generated in undoped crystals, and its intensity even exceeds that in the impurity region.

FWHM is an important parameter defining the sharpness of local levels in energy space. All emission bands in $CdGeP_2$ have comparable widths with a maximum ratio <7 [Fig. 5(b)]. Blue and/or violet pumping generates four more peaks than green pumping [15] and their FWHM are comparable or smaller. One of the narrow bands, as would be expected from the DOS, is located in the E_g region. The half-width of the principal line is ∼30 kT, which is larger than the characteristic parameter of interband and exciton lines [35,38]. Obviously, exciton emission from compensated $CdGeP_2$ crystals cannot be observed, so this broadening can be explained by large-scale modulation of the rms potential at the edges of continuum bands [20]. The effect on the DX centers is different and the formation of deep defect or impurity subbands in II-IV-V_2 cannot be ruled out.

Distribution histograms in Figs. 5(c) and 5(d) show the optical energy flows along different channels in the Mn-doped material. The most intense channels are 4, 5, 6, and 7 under green and blue excitation. Channels 12–16 become predominant under violet excitation. Interband transitions are observed only under short-wavelength pumping due to the participation of Mn^{2+} ions. Thus, electrons relax from intra-center Mn^{2+} levels to the CB edge of the $CdGeP_2$ matrix and further go into interband radiative recombination CB → VB. Such transitions are favored by the Mn^{2+}_{Ge} acceptor, which generates two holes per atom and is expected to have a shallow level or be located in the VB.

E. Energy-level diagram

Radiative transitions associated with point defects were detected in PL of the investigated $CdGeP_2$ crystals in the number of seven. The energy-level diagram for undoped $CdGeP_2$ is shown in Fig. 6; it brings together experimental data from this work and data from Refs. [15,19,30]. Belonging to donor and acceptor type is also in line with point defect calculations for $ZnGeP_2$ [25,26]. The Fermi level E_F is located below the middle band gap because the undoped $CdGeP_2$ crystal has p-type conductivity and N_A/N_D compensation.

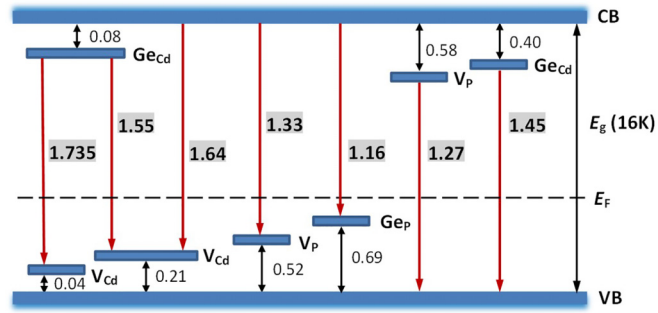

FIG. 6. Energy-level diagram and radiative transitions in undoped $CdGeP_2$ crystal. Energies of transitions are given in eV and rounded to 0.01 eV, $E_g = 1.852$ eV ($T = 16$ K).

According to calculations [24], anion-cation antisite defects Ge_P and P_{Ge} in $ZnGeP_2$ have low energies of formation and high concentrations of 10^{17}–10^{18} cm^{-3}. The modeling yielded an estimate comparable to that of the main dominant defect V_{Zn}. Since $ZnGeP_2$ crystals often exhibit an excess of Ge, and undoped $CdGeP_2$ and $ZnGeP_2$ are compensated and of p type (at least at low temperatures $T < 20$ K), we can attribute the observed 1.16 eV emission to a deep Ge_P acceptor involved in the CB → Ge_P transition. The deficit energy of 0.69 eV for this level is roughly 1/3 E_g in both $CdGeP_2$ and $ZnGeP_2$. The energy position of the level should be blurred due to two ionized charge states (-/0) that change relative to the Fermi level upon annealing or optical quenching. Among the 12 point defects calculated in Ref. [24], we cannot consider V_{Ge}, Zn_P, P_{Zn}, and P_{Ge} as unlikely point defects in terms of chemistry and crystal growth. The three interstitials Zn_i, Ge_i, and P_i are also unlikely due to their high energy of formation and therefore cannot be involved in the spectral analysis.

The first dominant point defect, Cd vacancy, in $CdGeP_2$ participates in three radiative transitions as shown in Fig. 6. One of them is the CB → V_{Cd} transition with the emission at 1.64 eV [Fig. 3(b)], and the energy deficit 0.21 eV. The acceptor activation energy of 0.20 eV for the V_{Cd} defect in undoped $CdGeP_2$ was found by a direct electrical measurement [30]. It was also shown that $CdGeP_2$ crystal is compensated, and the p type appears at low temperatures $T < 284$ K, but at room temperature the electric conductivity turns out to be n type. The two independent experiments from Refs. [20,30] are in good agreement for low-temperature p-type and high-temperature n-type undoped $CdGeP_2$.

The three defects V_{Cd}, Ge_{Cd}, and V_P were defined by EPR as one acceptor and two donors [19]. Their charge state can be switched by the 700 and 850 nm backlighting for the acceptor $V^{2-}_{Cd} \rightarrow V^{-}_{Cd}$, donor $Ge^{2+}_{Cd} \rightarrow Ge^{+}_{Cd}$, and donor $V^{+}_{P} \rightarrow V^{0}_{P}$. This means that photons with energy of about 1.77 and 1.459 eV activate paramagnetic centers with unpaired spins. Radiative transitions through the defect levels were found at 1.735 eV, and 1.45 eV under both excitations [Figs. 2(b) and 3(b)]. Optical absorption in the defect or impurity region can differ from emissions in experiments by a few meV. This small

violation of Kirchhoff's law is caused by the deviation from thermal equilibrium of the crystal during laser pumping. The situation is typical for II-IV-V_2 and other compound semiconductors. Thus, we ascribe these two emissions to the V_{Cd} acceptor and the Ge_{Cd} donor, respectively.

The transition at 1.735 eV is shown in the energy-level diagram (Fig. 6) as a transition of electron from shallow donor to shallow acceptor with a deficit of $0.08 + 0.04$ eV, although the absorption transition observed in Ref. [19] occurs slightly differently, 1.77 eV (80 K). This radiative transition is weak, whereas other alternative recombination channels with much higher DOS (CB and VB) provide optical transitions with higher probability.

The strongest PL emissions at 1.33, 1.45, and 1.55 eV taken in undoped and Mn-doped materials were also observed in In-, Ga-, and Cu-doped materials [17,18]. The first two transitions occur between the defect level and continuum band; the third D-A transition may be associated with the defect complex V_{Cd}-Ge_{Cd}-V_{Cd} forming with a very low energy similar to the V_{Zn}-Ge_{Zn}-V_{Zn} complex in $ZnGeP_2$ [25]. Mn doping helps the appearance of emissions through these levels, indicating the steadiness of the defects in more complex formations than single point defects.

The calculation in Ref. [26] predicts the V_P defect in $ZnGeP_2$ to be amphoteric with donor (-/0) and acceptor (0/-) levels at 0.6 ± 0.1 eV and 1.25 ± 0.1 eV above the VB, respectively. Chemical bonds in the chalcopyrite lattice of analogs are arranged by the same isostructural mode; therefore, we expect the phosphorus vacancy in $CdGeP_2$ forms the two D- and A-type levels in the gap. The radiative transitions at 1.27 and 1.33 eV (Fig. 6) can be tentatively attributed to this phosphorus vacancy in the donor and acceptor states. In addition, manganese as a source of extra holes suppresses the donor defects through Coulomb interaction or neutral pair formation, resulting in weaker emission intensity at 1.27 eV compared to 1.33 eV.

A special question remains about the Mn impurity level in the energy-level diagram. The preliminary electrical measurement of the Mn diffusion layer was conducted and obtained that the layer is of p type with the electrical conductivity σ higher by several orders of value compared to the undoped $CdGeP_2$ at $T = 300$ K. This indicates the Mn-related acceptor level is shallow (details will be reported in a separate publication). PL measurements do not allow distinguishing the Mn-related level among levels of multiple point defects in $CdGeP_2$:Mn. However, the theory performed for $Cd_{1-x}Mn_xGeP_2$ [32] confirmed that the isolated Mn_{Ge} defect generates a shallow acceptor level that is strongly spin polarized. The spin states are split such that the up-spin level is higher and the down-spin level is lower than the VBM.

IV. DISCUSSION

One of the minor emission bands is excited at 1.16 eV by the violet line, at 1.18 eV by the blue line, and at 1.195 eV by the green line. All three emission bands were attributed to the radiative transition from the CB to the acceptor level of the Ge_P anion-cation antisite. This Ge_P antisite exists because excess Ge is commonly observed in $CdGeP_2$ and $ZnGeP_2$, even in crystals of high optical quality. The concentration of this antisite defect was calculated for $ZnGeP_2$ as 10^{17}–10^{18} cm^{-3} [24]. The presence of this defect can lead to local strain around the Ge_P atom, since the tetrahedral covalent radii of Ge and P are 1.225 and 1.084 Å, respectively [55]. The radius difference of Ge and P atoms counts 12.2% and can lead to crystal instability. During the epitaxial growth of $CdGeP_2$, the lattice mismatch between the epilayer and GaAs substrate ($a = 5.741$ Å, $c/2 = 5.388$ Å, and $a = 5.653$ Å, respectively) can induce partial disorder and generate additional anion-cation antisites. Indeed, epitaxial growth is accompanied by the creation of an island structure, and the emission from the epilayer $CdGeP_2$ becomes much stronger at 1.195 eV [15]. Thus, the weak emission observed from the Mn diffusion layer indicates that Ge_P antisite defects also exist in $CdGeP_2$:Mn, but their concentration is low.

Defect complexes such as defect pairs and nanoclusters may play an important role, since the formation energy of defect pairs (Cd_{Ge}-Ge_{Cd}) is expected to be low, similar to the modeled pairs in the isostructural analogs $CuInSe_2$ [23] and $ZnGeP_2$ [25]. The radiative transition CB $\rightarrow V_{Cd}$ with a deficit of 0.21 eV can be alternatively considered as a transition associated with a defect complex ($2V_{Cd}^{-} - Ge_{Cd}^{2+}$), whose formation energy is very low [25]. We can go further by assuming a quasichemical reaction for three different point defects combined into a triple complex:

$$2V_{Cd}^{2-} + Ge_{Cd}^{2+} + V_P^{+} \rightarrow 2V_{Cd}^{-} + Ge_{Cd}^{+} + V_P^{0}. \qquad (3)$$

All three point defects V_{Cd} (acceptor), Ge_{Cd} (donor), and V_P (donor) exist in $CdGeP_2$ [19] and their formation energy is low (hence, high concentration) [25–27,32], so they contribute to the N_A/N_D compensation. Combining into triple complexes, Eq. (3), allows charged centers to exchange with electrons without violating local electroneutrality.

The electron exchange does not change the favorable conditions for the EPR signal, since the complex remains single charged (−), as shown in Eq. (3). Obviously, the exchange inside of the complex must be photoinduced and thermally specified. The formation of triple complexes should contribute to the reduction of the number of free carriers in the undoped crystal resulting in compensation. The known electron concentration in n-$CdGeP_2$ was measured as low as $(1.2–1.5) \times 10^{10}$ cm^{-3} at $T = 300$ K, and $N_A/N_D = 0.6 - 0.9$ [20]. In light of theoretical calculations performed in the last decade for compensated chalcopyrites, it can be assumed that the presence of triple complexes in p-$ZnGeP_2$ and p-$CdGeP_2$ is very likely at low temperatures.

The hole concentration in p-$CdGeP_2$ increases upon doping with Mn, and the charge exchange between point defects is greatly facilitated. This may be the reason for the stable emission and absorption observed at 1.64 eV. The hole transfer occurs at low temperatures (<18 K) and when the light is on. The initial charge state of the defects in the left part of Eq. (3) is stable at higher T and light off. In the right-hand side of Eq. (3), hole transfer is complete and the defects still have unpaired electron spins that produce the EPR signal. While the complex of defects ($2V_{Cd}^{-}$-Ge_{Cd}^{2+}) is confirmed by calculations, the existence of another complex of defects ($2V_{Cd}^{-}$-V_P^{0}) is unlikely, as this could lead to extended voids in the crystal lattice, which is low probability. The formation of a triple defect

complex (nanocluster) of the type ($2V_{Cd}^{-}$-Ge_{Cd}^{2+}-V_{P}^{0}) may be plausible with low energy of formation.

V. CONCLUSIONS

A series of radiative transitions in $CdGeP_2$ crystals, both undoped and Mn doped, was detected. One group of transitions is interpreted in terms of the participation of intrinsic point defects, which permanently exist in the crystalline material despite doping (Mn, In, Ga, Cu). The second group of transitions is related to Mn doping, which leads to two unusual effects: optical transitions through some defect levels are enhanced, including the interband transition, and high-energy optical transitions at $>E_g$, become dominant in the Mn-doped material. These two facts fundamentally distinguish Mn-doped ternary semiconductors II-IV-V_2 from their binary analogs III-V.

The structure of the *p*-like top valence bands in diamond-like compounds III-V and II-IV-V_2 is similar due to the same P and As anions. However, Mn dopes the crystal differently due to the acceptors Mn_{Ga} (one hole) and Mn_{Ge} (two holes), although both contribute to hole-mediated ferromagnetism. The energy band gap of undoped $CdGeP_2$ was determined, $E_g = 1.852$ eV (16 K), and an energy-level diagram for intrinsic point defects was proposed.

Radiative transitions at energies above the band gap proceed through Mn^{2+} ions and Mn^{2+} bound nanoclusters (quantum dots), which have already been observed in Mn-doped $CdGeP_2$ and $ZnGeP_2$ crystals. Manganese ions are easily incorporated into the chalcopyrite lattice without visible deformation of the crystal structure in both crystals. Introduction of Mn promotes the formation of Mn_{Cd} and Mn_{Ge} defects, while the diamondlike lattice of $CdGeP_2$ remains structurally well compatible with III-V compounds, germanium and silicon.

ACKNOWLEDGMENTS

The author would like to thank Professor K. Sato and Professor T. Ishibashi for the joint technology and Professor A. Toropov for assistance in measurements. This work was partially supported by the Innovation Promotion Fund FASIE, Project No. 3001p.

[1] H. P. Piyathilaka, R. Sooriyagoda, V. Dewasurendra, M. B. Johnson, K. T. Zawilski, P. G. Schunemann, and A. D. Bristow, Terahertz generation by optical rectification in chalcopyrite crystals $ZnGeP_2$, $CdGeP_2$ and $CdSiP_2$, Opt. Express **27**, 16958 (2019).

[2] B. N. Carnio, K. T. Zawilski, P. G. Schunemann, O. Moutanabbir, and A. Y. Elezzabi, The coming age of pnictide and chalcogenide ternary crystals in the terahertz frequency regime, IEEE Trans. Terahertz Sci. Technol. **12**, 433 (2022).

[3] G. A. Medvedkin, T. Ishibashi, T. Nishi, K. Hayata, Y. Hasegawa, and K. Sato, Room temperature ferromagnetism in novel diluted magnetic semiconductor $Cd_{1-x}Mn_xGeP_2$, Jpn. J. Appl. Phys. **39**, L949 (2000).

[4] K. Sato, G. A. Medvedkin, T. Nishi, Y. Hasegawa, R. Misawa, K. Hirose, and T. Ishibashi, Ferromagnetic phenomenon revealed in the chalcopyrite semiconductor $CdGeP_2$:Mn, J. Appl. Phys. **89**, 7027 (2001); G. A. Medvedkin, T. Ishibashi, T. Nishi, and K. Sato, New magnetic semiconductor $Cd_{1-x}Mn_xGeP_2$, Semiconductors **35**, 291 (2001).

[5] K. Sato, G. A. Medvedkin, T. Ishibashi, and K. Hirose, Room temperature ferromagnetism in the novel magnetic semiconductors based on II-IV-V_2 chalcopyrite compounds, J. Cryst. Growth **237–239**, 1363 (2002); K. Sato, G. A. Medvedkin, T. Ishibashi, S. Mitani, K. Takanashi, Y. Ishida, D. D. Sarma, J. Okabayashi, A. Fujimori, T. Kamatani, and H. Akai, Novel Mn-doped chalcopyrites, J. Phys. Chem. Solids **64**, 1461 (2003).

[6] G. A. Medvedkin and V. G. Voevodin, Magnetic and optical phenomena in nonlinear optical crystals $ZnGeP_2$ and $CdGeP_2$, J. Opt. Soc. Am. B **22**, 1884 (2005).

[7] G. A. Medvedkin, Yu. V. Rud, M. A. Tairov, and Yu. K. Undalov, Photoelectric properties of structures based on $CdGeP_2$ and its binary analog InP, Zh. Tekhn. Fiz. **60**, 174 (1990).

[8] G. A. Medvedkin, Yu. V. Rud, and M. A. Tairov, Photoelectric anisotropy of II-IV-V_2 ternary semiconductors, Phys. Status Solidi A **115**, 11 (1989).

[9] M. van Schilfgaarde, T. J. Coutts, N. Newman, and T. Peshek, Thin film tandem photovoltaic cell from II-IV-V chalcopyrites, Appl. Phys. Lett. **96**, 143503 (2010).

[10] A. D. Martinez, A. N. Fioretti, E. S. Tobererab, and A. C. Tamboli, Synthesis, structure, and optoelectronic properties of II-IV-V_2 materials, J. Mater. Chem. A **5**, 11418 (2017).

[11] M. Pandey, K. Kuhar, and K. W. Jacobsen, II-IV-V_2 and III-III-V_2 polytypes as light absorbers for single junction and tandem photovoltaic devices, J. Phys. Chem. C **121**, 17780 (2107).

[12] D. H. Fabini, M. Koerner, and R. Seshadri, Candidate inorganic photovoltaic materials from electronic structure-based optical absorption and charge transport proxies, Chem. Mater. **31**, 1561 (2019).

[13] *Spintronics Handbook, Second Edition, Spin Transport and Magnetism*, edited by E. Y. Tsymbal and I. Žutić, Semiconductor Spintronics Vol. 2 (CRC Press, Boca Raton, FL, 2019).

[14] G. A. Medvedkin, S. I. Goloshchapov, V. G. Voevodin, K. Sato, T. Ishibashi, S. Mitani, K. Takanashi, A. Fujimori, Y. Ishida, J. Okabayashi, D. D. Sarma, H. Akai, and T. Kamatani, Novel spintronic materials based on ferromagnetic semiconductor chalcopyrites, Int. J. Nanosci. **3**, 39 (2004).

[15] G. A. Medvedkin, V. M. Smirnov, T. Ishibashi, and K. Sato, Photoluminescence of $CdGeP_2$ and $(Cd, Mn)GeP_2$, J. Phys. Chem. Solids **66**, 2015 (2005).

[16] H. Boudriot and H. A. Schneider, Anwendungsmoglichkeiten von II-IV-V_2 halbleitern auf dem gebiet der optoelektronik, Acta Phys. Acad. Sci. Hungaricae **51**, 361 (1981) [in German].

[17] I. A. Maltseva, A. Mamedov, Yu. V. Rud, and Yu. K. Undalov, Luminescence of In-doped $CdGeP_2$ crystals, Phys. Status Solidi A **50**, 139 (1978).

[18] N. A. Goryunova, S. M. Ryvkin, G. P. Shpenikov, I. I. Tichina, and V. G. Fedotov, Investigations of some properties of vitreous and crystalline $CdGeP_2$, Phys. Status Solidi **28**, 489 (1968).

[19] T. D. Gustafson, N. C. Giles, P. G. Schunemann, K. T. Zawilski, K. L. Averett, J. E. Slagle, and L. E. Halliburton, Intrinsic point defects (vacancies and antisites) in $CdGeP_2$ crystals, J. Appl. Phys. **133**, 245703 (2023).

[20] G. A. Medvedkin, Yu. V. Rud, and M. A. Tairov, Anisotropy of the optical absorption edge in compensated n-$CdGeP_2$ crystals, Fiz. Tekhn. Poluprov., **24**, 1306 (1990).

[21] I. H. Choi, D. H. Lee, Y. D. Choi, Y. M. Yu, and P. Y. Yu, Optical and vibrational properties of the chalcopyrite $CdGeP_2$, J. Korean Phys. Soc. **44**, 403 (2004).

[22] S. Lany and A. Zunger, Intrinsic DX centers in ternary chalcopyrite semiconductors, Phys. Rev. Lett. **100**, 016401 (2008).

[23] S. B. Zhang, S.-H. Wei, A. Zunger, and H. Katayama-Yoshida, Defect physics of the $CuInSe_2$ chalcopyrite semiconductor, Phys. Rev. B **57**, 9642 (1998); Stabilization of ternary compounds via ordered arrays of defect pairs, Phys. Rev. Lett. **78**, 4059 (1997).

[24] M. Huang, S.-S. Wang, Y.-N. Wu, and S. Chen, Defect physics of ternary semiconductor $ZnGeP_2$ with a high density of anion-cation antisites: A first-principles study, Phys. Rev. Appl. **15**, 024035 (2021).

[25] X. Jiang, M. S. Miao, and W. R. L. Lambrecht, Theoretical study of cation-related point defects in $ZnGeP_2$, Phys. Rev. B **71**, 205212 (2005).

[26] X. Jiang, M. S. Miao, and W. R. L. Lambrecht, Theoretical study of the phosphorus vacancy in $ZnGeP_2$, Phys. Rev. B **73**, 193203 (2006).

[27] X. Jiang, M. S. Miao, and W. R. L. Lambrecht, Electronic structure of native point defects in $ZnGeP_2$, Mater. Res. Soc. Symp. Proc. **799**, Z5.3.1 (2004).

[28] G. Medvedkin, Optical dichroism in $ZnGeP_2$ crystals at deep levels, J. Opt. Soc. Am. B **39**, 851 (2022).

[29] K. Somogyi and I. Bertoti, Some electrical properties of $ZnGeP_2$ crystals, Jpn. J. Appl. Phys. **11**, 103 (1972).

[30] A. Miller and W. Clark, Electrical properties of $ZnGeP_2$ and $CdGeP_2$, J. Phys. Colloq. **36**, C3-73 (1975).

[31] H. M. Hobgood, T. Henningsen, R. N. Thomas, R. H. Hopkins, M. C. Ohmer, W. C. Mitchel, D. W. Fischer, S. M. Hegde, and F. K. Hopkins, $ZnGeP_2$ grown by the liquid encapsulated Czochralski method, J. Appl. Phys. **73**, 4030 (1993).

[32] P. Mahadevan and A. Zunger, Room-temperature ferromagnetism in Mn-doped semiconducting $CdGeP_2$, Phys. Rev. Lett. **88**, 047205 (2002); **88**, 159904(E) (2002).

[33] V. V. Popov and G. A. Medvedkin, Hole transport anomaly in high-T_C ferromagnet (Zn, Mn)GeP_2, Solid State Commun. **132**, 561 (2004).

[34] G. A. Medvedkin, V. V. Popov, S. I. Goloshchapov, P. G. Baranov, H. Blok, S. B. Orlinskii, and J. Schmidt, Study of magnetic clusters in the system ferromagnetic-nonmagnetic semiconductors (Zn, Mn)GeP_2/$ZnGeP_2$ by means of hole transport and magnetic resonance, in *Proceedings of the 13th International Symposium on Nanostructures: Physics and Technology* (Ioffe Institute, St. Petersburg, Russia, 2005), pp. 149–150.

[35] G. A. Medvedkin, T. Nishi, and K. Sato, Photoluminescence of $CdSnP_2$ single crystals in the vicinity of the fundamental optical edge, Jpn. J. Appl. Phys. **39**, 6301 (2000).

[36] K. Furdyna, Diluted magnetic semiconductors, J. Appl. Phys. **64**, R29 (1988).

[37] *Introduction to the Physics of Diluted Magnetic Semiconductors*, edited by J. Kossut and J. A. Gaj (Springer, Berlin, 2010).

[38] J. L. Shay and J. H. Wernick, *Ternary Chalcopyrite Semiconductors: Growth, Electronic Properties, and Applications* (Pergamon Press, New York, 1975).

[39] P. G. Baranov, S. I. Goloshchapov, G. A. Medvedkin, and V. G. Voevodin, Detection of magnetic resonance signals with anomalous dispersion and two types of isolated manganese centers in the chalcopyrite crystal (Zn, Mn)GeP_2, JETP Lett. **77**, 582 (2003).

[40] T. Kamatani and H. Akai, Electronic structure and magnetism of novel diluted magnetic semiconductors $CdGeP_2$:Mn and $ZnGeP_2$:Mn, Phase Trans. **76**, 401 (2003).

[41] H. Yi and H. Park, Electronic structure and half-metallic ferromagnetism in $CdGe_{1-x}Mn_xP_2$, chalcopyrite semiconductor, J. Korean Phys. Soc. **45**, S530 (2004).

[42] P. G. Baranov, S. I. Goloshchapov, G. A. Medvedkin, V. G. Voevodin, S. B. Orlinskii, and J. Schmidt, Giant electron spin echo of ferromagnetic ordered manganese nanoclusters in (Zn, Mn)GeP_2 crystals, in *Proceedings of the 12th International Symposium on Nanostructures: Physics and Technology* (Ioffe Institute, St. Petersburg, Russia, 2004), pp. 28–29.

[43] L. Hong-Ganga, W. Xiao-Xuan, and Z. Wen-Chen, Zero-field splittings and local tilting angles τ_{Mn2+} for Mn^{2+} in $ZnGeP_2$ and $CdGeP_2$ crystals, Spectrachem. Acta A **71**, 417 (2008).

[44] N. Nateghi, S. Lambert-Milot, and R. A. Masut, Epitaxial to axiotaxial texture evolution in endotaxial MnP films grown on GaP (100), J. Vac. Sci. Technol. A **38**, 033412 (2020).

[45] S. Lambert-Milot, S. Gaudet, C. Lacroix, D. Ménard, R. A. Masut, C. Lavoie, and P. Desjardins, MnP nanoclusters embedded in GaP epitaxial films grown by organometallic vapor-phase epitaxy: A reciprocal space mapping and transmission electron microscopy study, J. Vac. Sci. Technol. A **30**, 061510 (2012).

[46] G. Monette, N. Nateghi, R. A. Masut, S. Francoeur, and D. Ménard, Plasmonic enhancement of the magneto-optical response of MnP nanoclusters embedded in GaP epilayers, Phys. Rev. B **86**, 245312 (2012).

[47] C. Lacroix, S. Lambert-Milot, R. A. Masut, P. Desjardins, and D. Ménard, Ferromagnetic resonance measurements of GaP epilayers with embedded MnP nanoclusters grown on GaP(001), Phys. Rev. B **87**, 024412 (2013).

[48] C. Lacroix, S. Lambert-Milot, P. Desjardins, R. A. Masut, and D. Ménard, Magnetic anisotropy in GaP(001) epilayers containing MnP nanoclusters observed by angle dependent ferromagnetic resonance measurements, J. Appl. Phys. **103**, 07D531 (2008).

[49] Th. Hartmanna, M. Lampalzer, P. J. Klar, W. Stolz, W. Heimbrodt, H.-A. Krug von Nidda, A. Loidl, and L. Svistov, Ferromagnetic resonance studies of (Ga,Mn)As with MnAs clusters, Physica E **13**, 572 (2002).

[50] K. S. Burch, D. D. Awschalom, and D. N. Basov, Optical properties of III-Mn-V ferromagnetic semiconductors, J. Magn. Magn. Mater. **320**, 3207 (2008).

[51] P. Mahadevan and A. Zunger, Ferromagnetism in Mn-doped GaAs due to substitutional-interstitial complexes, Phys. Rev. B **68**, 075202 (2003).

[52] Y. P. Varshni, Temperature dependence of the energy gap in semiconductors, Physica **34**, 149 (1967).

[53] S. C. Abrahams and F. S. L. Hsu, Debye temperatures and cohesive properties, J. Chem. Phys. **63**, 1162 (1975).

[54] *Semiconductors* $A^2B^4C_2^5$, edited by N. A. Goryunova and Yu. A. Valov (Soviet Radio, Moscow, 1974) [in Russian].

[55] P. Pyykkö, Refitted tetrahedral covalent radii for solids, Phys. Rev. B **85**, 024115 (2012).